

Article

# Gain Measurement of ZnGeP<sub>2</sub> Optical Parametric Oscillator Pulses in a High-Pressure CO<sub>2</sub> Amplifier

Ziren Zhu <sup>1,2</sup> , Yu Liu <sup>1,2</sup>, Jinghan Ye <sup>1,2</sup>, Juntao Tian <sup>1,2</sup>, Tianjian Wan <sup>1,2</sup>, Jinzhou Bai <sup>1,2</sup>, Yijun Zheng <sup>1,2,\*</sup>, Rongqing Tan <sup>1,2,\*</sup>, Zhiyong Li <sup>1</sup> and Xinjun Su <sup>3</sup>

<sup>1</sup> Aerospace Information Research Institute, Chinese Academy of Sciences (AIRCAS), Beijing 100094, China; zzzr@aircas.ac.cn (Z.Z.); liuyu211@mails.ucas.ac.cn (Y.L.); zhiyongli@aircas.ac.cn (Z.L.)

<sup>2</sup> University of Chinese Academy of Sciences (UCAS), Beijing 100049, China

<sup>3</sup> National Laboratory of Science and Technology on Particle Transport and Separation (NLPTS), Tianjin 300180, China

\* Correspondence: zhengyj@aircas.ac.cn (Y.Z.); tanrq@aircas.ac.cn (R.T.)

**Abstract:** Laser pulse amplification by a high-pressure CO<sub>2</sub> amplifier in the long-wave infrared (LWIR) spectral range is a feasible technology for strong-field physics research. Crystals such as ZnGeP<sub>2</sub> (ZGP) have high nonlinear coefficients and transmittance in the LWIR region, with spectral widths of generated pulses closely matching the gain spectrum of high-pressure CO<sub>2</sub> amplifiers. Therefore, ZGP optical parametric oscillation (OPO) may allow higher-efficiency energy extraction in amplifiers, improving the output characteristics of LWIR amplification systems. In this study, the gain measurement of ZGP OPO pulses amplified by a high-pressure CO<sub>2</sub> amplifier was carried out for the first time. Single-detector acquisition was utilized to achieve a unified sensor responsivity, and a laser signal-triggered function generator was used to synchronize the seed pulse and amplifier. Six-pass amplification was performed successively, yielding an amplification factor of 4.5 for the peak power and a maximum coefficient of 0.42% cm<sup>-1</sup> for the small-signal gain. The gain and loss effect during small-signal amplification were discussed. The potential capability of acquiring ultra-short pulses with ZGP OPO pulses was also explored with the FFT function of MATLAB software.

**Keywords:** high-pressure CO<sub>2</sub> amplifier; optical parametric oscillator; ZnGeP<sub>2</sub>; small-signal gain



**Citation:** Zhu, Z.; Liu, Y.; Ye, J.; Tian, J.; Wan, T.; Bai, J.; Zheng, Y.; Tan, R.; Li, Z.; Su, X. Gain Measurement of ZnGeP<sub>2</sub> Optical Parametric Oscillator Pulses in a High-Pressure CO<sub>2</sub> Amplifier. *Photonics* **2024**, *11*, 154. <https://doi.org/10.3390/photonics11020154>

Received: 6 January 2024

Revised: 30 January 2024

Accepted: 3 February 2024

Published: 5 February 2024



**Copyright:** © 2024 by the authors. Licensee MDPI, Basel, Switzerland. This article is an open access article distributed under the terms and conditions of the Creative Commons Attribution (CC BY) license (<https://creativecommons.org/licenses/by/4.0/>).

## 1. Introduction

Long-wave infra-red (LWIR) technologies and their applications have been developing rapidly in recent years. Optical parametric oscillation (OPO) is an oscillator based on nonlinear optical effects that produces laser beams with tunable frequencies. The basic principle of a difference frequency generation (DFG) process is to convert the input laser light (often called pumping light) into a lower frequency signal light and a higher frequency idler light through nonlinear optical interaction. The sum of the frequencies of the two outputs is equal to the frequency of the input light. J. Yuan reported a CdSe OPO operating at 12.07 μm at a pulse repetition frequency of 1.2 kHz pumped with a Q-switched Ho:YAG laser. The idler wavelength from the CdSe OPO could be tuned from 10.24 to 12.07 μm [1,2]. C. Qian reported a ZnGeP<sub>2</sub> (ZGP) OPO pumped with a three-stage Ho:YAG master oscillator power amplifier (MOPA). The maximal average output powers were 3.15 W at 8.2 μm and 11.4 W at 2.8 μm [3]. K. Yang demonstrated a non-critical phase-matching BaGa<sub>4</sub>Se<sub>7</sub> OPO pumped with a Q-switched Ho: YLF laser. The idler output tuning range was from 9.3 to 10.6 μm, which matched well with the gain spectrum of four bands of a CO<sub>2</sub> amplifier [4,5]. However, there is still potential for such OPO devices to achieve a higher output power or pulse energy due to the limited coating damage threshold at present.

CO<sub>2</sub> molecules can achieve continuous gain in four bands (9R, 9P, 10R, and 10P) from 9 to 11 μm at a high pressure due to the pressure broadening effect [6–9]. Thus, a high-pressure CO<sub>2</sub> amplifier with a large gain volume is able to avoid laser-induced damage

at a relatively low power density and realize the amplification of OPO pulses mentioned above. However, few reports on the experimental amplification of nonlinear crystal OPO pulses with high-pressure CO<sub>2</sub> amplifiers have been revealed so far. A similar LWIR MOPA system of Brookhaven National Laboratory (BNL) has become available in high-energy physics and material research [10–13]. Seed pulses at 9.2 μm were generated in a setup comprising an Erbium oscillator, Ti:Sapphire laser amplifier, and an optical parametric amplification (OPA)-based frequency conversion device. Two high-pressure, mixed-isotope CO<sub>2</sub> amplifiers were used to amplify the pulse to up to 20 J successively. The US Naval Research Laboratory and Air Force Research Laboratory also proposed a terawatt-class CO<sub>2</sub> laser based on an injection-seeded unstable resonator concept [14]. The ~10 μm wavelength was designed in a DFG GaSe crystal driven by solid-state OPA system. Moreover, such a combination of solid and gaseous laser systems has prospective applications in LWIR lidar detection and atmospheric optical communications. A continuously tunable and wide output frequency range is able to cover the absorption peaks of many molecules and a number of atmospheric windows.

According to the survey, this study is the first trial of the amplification of ZGP OPO pulses by a high-pressure CO<sub>2</sub> amplifier. The small-signal gain coefficient was measured. Characteristics and expectations of such pulses were also discussed here.

## 2. Experiment

### 2.1. Experimental Setup

The experimental setup is shown in Figure 1. The seed pulses were generated using a ZGP OPO that was constructed in-house [15]. The oscillator was pumped using a 23.03 W Q-switched Ho:YAG laser with a wavelength of 2.1 μm and a type-I phase matching angle. The pulse width of the pump source was ~25 ns.

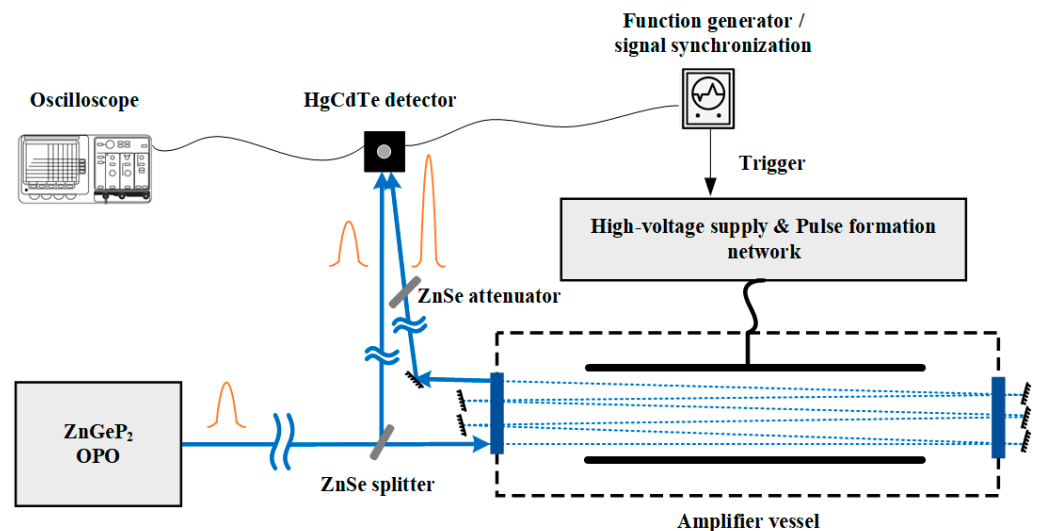


**Figure 1.** Setup of the ZGP OPO pulse amplification experiment.

The ZGP crystal was cut at 51.5 deg. The central wavelength of 9.27 μm was achieved at the phase-matching angle of 51.06 deg, corresponding to a region of relatively high gain in the CO<sub>2</sub> spectrum. The maximum average idler output power was 1.2 W at a repetition frequency of 10 kHz. The beam diameter was 5 mm. The pulse waveform is shown in Figure 2a. Using a HgCdTe detector with multi-stage signal amplification (Thorlabs MCT, Newton, MA, USA), the full width at half maximum (FWHM) of the temporal waveform was measured to be 35 ns and the spectral width was ~110 nm.

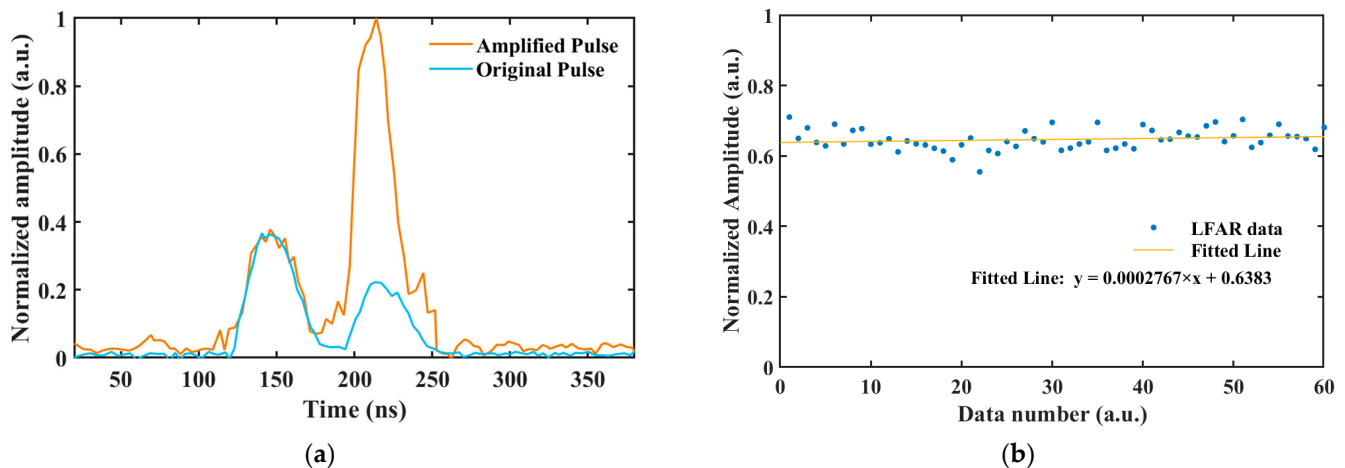


**Figure 2.** (a) Waveforms of pulse pairs with (orange) or without (blue) the existence of discharge at detector gain level 6; (b) amplitude ratio of original pulse pairs without amplification (dots) and fitting with an approximately horizontal distribution (line).

The amplifier was transversely excited at a repetition frequency of 0.25 Hz and a voltage of 70 kV. It had an active volume of 20 mm × 20 mm × 600 mm and was UV-preionized. The pressure of the mixture inside the amplifier was 4 atm, and the mixture ratio of CO<sub>2</sub>:N<sub>2</sub>:He was 1:1:10. The discharge was triggered by external signals with a time delay of 95.35 μs.

The collimated seed pulses were split using a filmed ZnSe plate (reflectivity of 15%) placed in front of the amplifier. The reflected part was directly sent into the HgCdTe detector, and the residual part was injected into the high-pressure CO<sub>2</sub> amplifier. After six-pass traversal, the temporal signal of the amplified pulse was attenuated using a filmed ZnSe plate (transmittance of 20%) and collected by the same HgCdTe detector. Thus, the waveforms of pulse pairs with a fixed time delay were obtained, as shown in Figure 2a. Due to unavoidable diffraction loss and transmission loss during the multi-pass, the amplitude of the latter pulse in the pair was lower than the former one.

In order to reduce most of the electromagnetic interference (EMI) caused by the discharge of the CO<sub>2</sub> amplifier, several countermeasures were taken: a Faraday cage and an isolated battery power supply for the detector and the oscilloscope and earthing of the shielding layer of cables and fiber isolated trigger circuit. Even so, tiny EMI still penetrated through apertures and was captured on the oscilloscope image, which shall be discussed later.

## 2.2. Acquisition Method

For analyzing the amplification behavior synchronously in a one-shot process, common acquisition methods involve several detectors placed before and after the amplifier. These methods perform detailed measurements while introducing potential nonuniformity in response characteristics between detectors. In this study, a one-detector acquisition method based on the difference between two optical paths was utilized. The detector delivered output voltage signals proportional to the intensities of the optical signals at different gains (levels 1–8) according to the sensor specifications provided by Thorlabs. This approach unified the sensor responsivity, which was beneficial for evaluating the amplification via comparison and avoiding display saturation in our observation tool—a digital oscilloscope (Tektronix 4104B, Beaverton, OR, USA).

## 2.3. Time Sequence

As the ZGP OPO device was not designed for an external trigger mode, the time sequence was established on the timeline of periodic OPO pulse signals. Two adjacent seed pulse signals (former signal A and latter signal B, duration 100 μs) acquired by the HgCdTe

detector were involved in one shot process. Signal A was used for triggering the function generator, and the function generator then triggered the amplifier discharge to match the amplification gain and signal B. A function generator (Agilent 81150A, Mississauga, Canada) was triggered by fast-clock seed pulses in each cycle  $T = 100 \mu\text{s}$ , and it sent slow-clock trigger signals to control the amplifier discharge in each cycle  $T' = 4 \text{ s}$  with an additional delay (AD). By adjusting the AD manually, the seed pulse matched the temporal gain of the  $\text{CO}_2$  amplifier successfully.

### 3. Results and Discussions

#### 3.1. Amplification Effect

By controlling the discharge, the comparison of waveforms with and without amplification was achieved. The blue curve in Figure 2a represents the original waveforms of pulse pairs without amplification at detector gain level 6 ( $-4.2 \text{ dB}$ ). The first pulse was a sample of the original pulse, whereas the second pulse was the pulse that passed through the vessel. The two pulses have the same shape, with a width of  $35 \text{ ns}$ . The latter-to-former-amplitude ratio (LFAR) was  $61.8\%$ , as determined by the ratio of the splitter, attenuator, diffraction, etc. This contrast in waveforms was set up merely as a criterion case without amplification. The stability of the measured amplitude ratio of pulse pairs is shown in Figure 2b. The calculated average amplitude ratio was  $0.65$ , and the standard deviation was  $0.0048$ , which was only  $0.7\%$  of the average value. Despite small random deviations in the ratios, the fitted slope remained at a near-zero level, indicating that the single-detector acquisition method based on the optical path difference allowed for an intuitive amplification analysis.

Figure 2a also shows the waveform of the pulse pair with the amplification effect. A comparison with the criterion case without amplification revealed that there were irregular noises near the ground line, which could be explained as EMI caused by amplifier discharge or the amplified stray optical signal. The LFAR after amplification was  $275.6\%$ . The pulse width after amplification was  $28.4 \text{ ns}$ . A maximum amplification factor of  $275.6\%/61.8\% = 4.5$  in LFAR and a reduction ratio of  $18.4\%$  in the pulse width were achieved. The maximum small-signal gain was  $0.42\% \text{ cm}^{-1}$  corresponding to a utilization efficiency (UE) of  $\sim 48\%$  of the gain spectrum by integral area in Figure 3b.

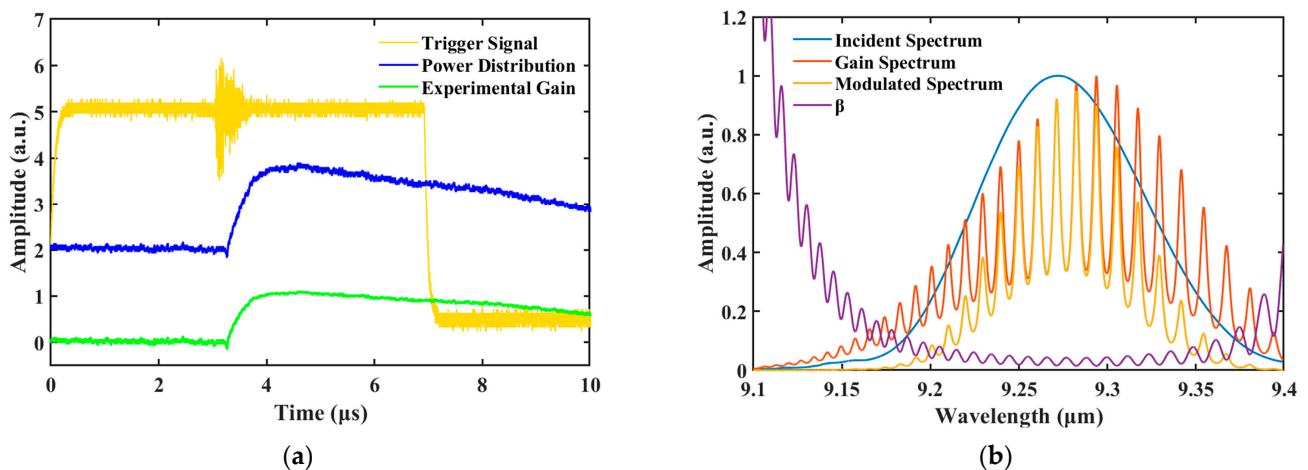


**Figure 3.** (a) Temporal power distribution, gain distribution, and the rising edge of a trigger signal; (b) normalized distribution of the incident spectrum, the gain spectrum, the spectrum modulated via multiplication of the incident spectrum and the gain spectrum, and the ratio  $\beta$  of the absorption coefficient to the gain coefficient at a mixture pressure of  $4 \text{ atm}$ .

#### 3.2. Gain and Loss of Laser Power in Discharge Region

By replacing ZGP OPO with a tunable CW  $\text{CO}_2$  laser, the temporal distributions of amplifier trigger signal and amplified laser power were measured and plotted in Figure 3a.

Experimental and theoretical gain coefficients were calculated according to (1) and (2) separately [16]:

$$G_{\text{experimental}} = \ln\left(\frac{P_{\text{max}}}{P_{\text{CW}}}\right) / L_{\text{gain}} \quad (1)$$

$$G_{\text{theoretical}} = N_{\text{upper}}\sigma_{\text{upper}} - N_{\text{lower}}\sigma_{\text{lower}} \quad (2)$$

where  $P_{\text{max}}$  is the maximum value of the amplified power curve and  $P_{\text{CW}}$  is the mean power without the amplification effect.  $L_{\text{gain}}$  is the gain length.  $N$  and  $\sigma$  represent number densities and collision sections of the upper level and lower level, respectively.

With the method of CW laser amplification, the measured maximum gain coefficient in the 9R branch ( $1.11\% \text{ cm}^{-1}$  at wavelength  $9.27 \mu\text{m}$ ) was determined. Moreover, the ZGP OPO pulse injection moment is at the top of the experimental gain coefficient curve in Figure 3a. The normalized spectral gain distribution is shown in Figure 3b. The seed pulse spectrum data were obtained using a Fourier transform infrared spectrometer [14], whereas the gain spectrum was calculated theoretically using the six-temperature model [16]. Comparing  $G_{\text{experimental}}$  with  $G_{\text{theoretical}}$ , such a low gain coefficient of a large frequency range may result from the deep modulation effect at a relatively low pressure and the mismatch of  $\sim 0.02 \mu\text{m}$  between the central wavelength of the seed spectrum and gain spectrum.

The loss effect inferred as the continuum radiation absorption coefficient [17] of plasma at temperature  $T$  and incident beam frequency  $\nu$  may be approximated as follows:

$$K(\nu) = 0.0177\bar{z}\nu^{-2}N_e^2T^{-3/2} \cdot \eta \quad (3)$$

For plasma in  $\text{CO}_2$  lasers and amplifiers that was predominantly singly ionized, the charge value was  $\bar{z} = 1$ . The estimated electron density value was  $N_e \approx 2 \times 10^{14} \text{ cm}^{-3}$  (seed pulse incident moment). The coefficient  $\eta$  may be 1.5 at the assumed plasma temperature  $T \approx 2 \times 10^3 \text{ K}$ . The calculated  $K(\nu)$  at a frequency of  $32.33 \text{ THz}$  ( $9.27 \mu\text{m}$ ) was  $1.1 \times 10^{-5} \text{ cm}^{-1}$ . By defining the absorption/gain ratio  $\beta$ , the distribution of  $\beta$  with respect to the wavelength was plotted, as shown in Figure 3b.  $\beta$  remained at a relatively low level ( $<10\%$ ) in the central part of the 9R branch. It gradually increased as the wavelength varied to the margin and approached the gain coefficient. These data characteristics may indicate asymmetric frequency distortion during pulse amplification, as marginal frequencies were completely cut off.

The discussions above mainly described the gain distribution in the frequency domain. However, no chirp was introduced in this setup during amplification. The compression in pulse width after multi-pass amplification could be clarified as the loss of marginal temporal parts of the seed corresponding with a negative net gain factor. Assuming that the pulse shape was a symmetric type corresponding to a peak power of  $3 \times 10^3 \text{ W}$  and a pulse width of  $35 \text{ ns}$ , signal power under  $\sim 270 \text{ W}$  ( $\sim 9\%$  of peak power) vanished during amplification. The estimated plasma absorption loss factor was  $-0.26\% \text{ cm}^{-1}$  according to the calculation form in (1). In other words, the analysis of pulse width compression of small-signal seed pulses provided a measurement of laser radiation absorption by plasma.

### 3.3. Phase Shift and Power Spectrum

The phase shift in a low-density plasma could be expressed as (4) according to the Drude model [18] and Eli Yablonovitch's method [19]:

$$\phi = -\left\{1 - [1 - N_e(t)/N_c]^{1/2}\right\}z\omega/c \quad (4)$$

where the first square bracket represents the variation in the refractive index caused by the absorption of plasma.  $z$  represents the propagation path length and  $\omega = 2\pi\nu$  is the circular frequency of the pulse.  $N_c = m\omega^2/4\pi e^2$  is the critical density at which the plasma frequency equals the laser frequency and the plasma could be fully opaque to laser radiation.  $m$  represents the mass of the electron.

By taking the Fourier transform of (4), the power spectrum was obtained analytically:

$$P_A = (T_a/\omega') \{ \exp[(\pi - 2\theta)\omega'T_a] - \exp[-(\pi + 2\theta)\omega'T_a] \} \quad (5)$$

where  $T_a \approx -1.4 \times 10^{-6}$  is defined in  $N_e(t) = N_{e,t=incident}e^{t/T_a}$ , which describes the decline in the electron density within microseconds in Figure 4a.  $\omega'$  represents the frequency shift from the line center.  $\theta \approx \arctan \phi$  was calculated as  $\phi \approx -49.75$  rad according to (4). The calculated power spectrum after the total six-pass amplification was plotted in Figure 4b. In contrast to plasma generated by a rapid laser-breakdown process,  $N_e(t)$  declined within a few microseconds. Nonetheless, in the duration of pulse amplification lasting dozens of nanoseconds, the electron density underwent minor changes, and the theoretical phase shift in the plasma is quasi-symmetric relative to the central frequency. The fall-off on the anti-Stokes side was as fast as that on the Stokes side. Summarizing the discussions in Sections 3.2 and 3.3, the plasma absorption and plasma-induced phase shift of the incident pulse both had an influence on the amplitude and the frequency distribution. As the broadening in the power spectrum ( $\ll 1$  MHz) occupied a minor scale compared with the line width of the seed pulse ( $>100$  GHz), the plasma absorption effect dominated the pulse width compression.

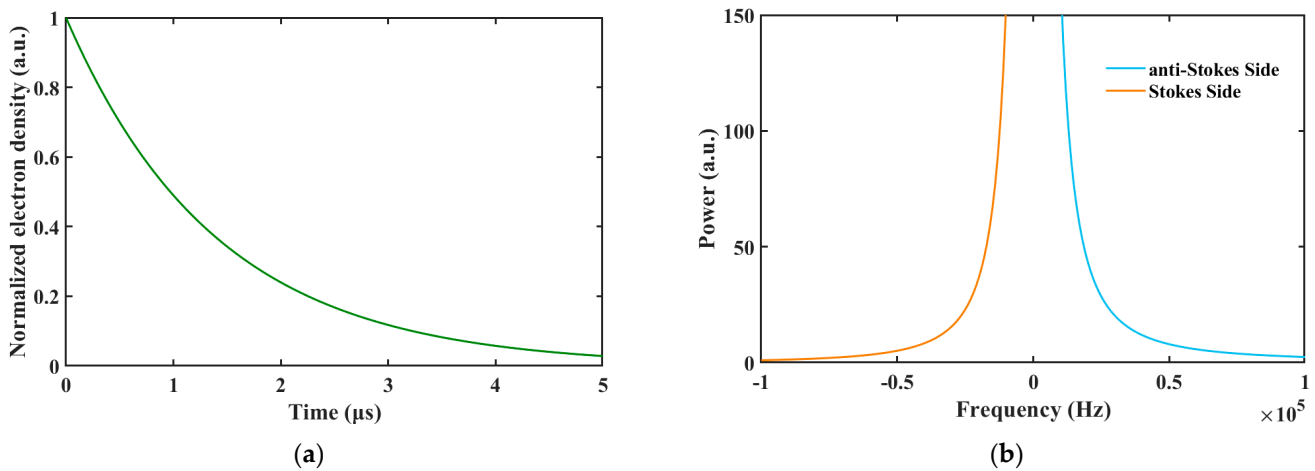


**Figure 4.** (a) Temporal distribution of electron density of amplifier discharge; (b) power spectrum as a consequence of phase shift.

### 3.4. Potential Application in Ultrashort Pulse Amplification

The measured maximum small-signal gain in Section 3.1 was not ideal compared with TEA CO<sub>2</sub> MOPA systems with a narrow linewidth. However, a higher mixture pressure in CO<sub>2</sub> may make better use of the wide linewidth and improve the gain coefficient. Theoretical explanations of the effect of spectrum matching at different mixture pressures are shown in Figure 5a. At higher mixture pressures, there was a noticeable reduction in the modulation depth owing to the collision broadening effect. UE values corresponding to 4, 6, and 8 atm were 48%, 61%, and 83% respectively. The Fast Fourier Transformation (FFT) function of the modulated spectrum as a function of the workable amplifier pressure is presented in Figure 5b with MATLAB software. A pulse train shape similar to that reported in a previous work was observed with a fixed pulse-to-pulse duration of 12.8 ps as a consequence of spectral modulation, which had been clarified elsewhere [6,11]. The primary pulse FWHM was 1.45 ps. However, a higher pressure contributed to a decrease in the energy fraction of sub-pulses. The estimated amplitude contrast ratio between the primary pulse and adjacent sub-pulse was 1000:55 at a pressure of 8 atm. These findings suggest that a picosecond slice of a ZGP OPO pulse may be applicable to LWIR amplification with a similar experimental setup in BNL [12]. More detailed simulations of realizing picosecond

terawatt pulses with chirped amplification LWIR systems may be carried out in a future work after careful setup design and sufficient parametric optimization.

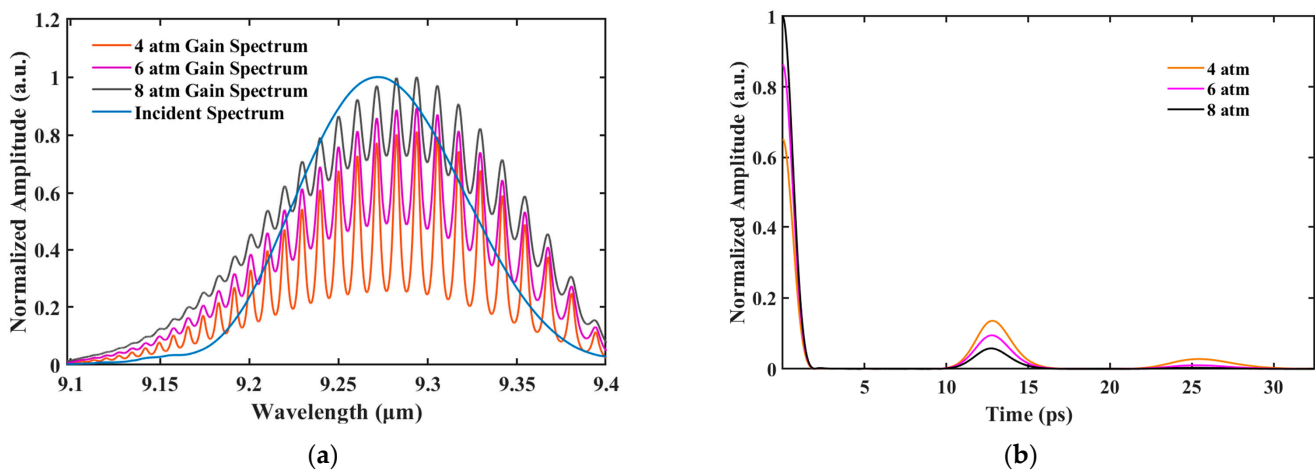


**Figure 5.** (a) Spectral distribution of incident pulse (blue); gain coefficient with different mixture pressures, 8 atm (black), 6 atm (pink), 4 atm (orange). (b) The FFT figure of the modulated spectrum (multiplication of gain spectrum and incident spectrum) with different mixture pressures.

#### 4. Conclusions

In this study, the ZGP OPO pulse gain coefficient in a CO<sub>2</sub> amplifier at a pressure of 4 atm was measured for the first time. This was achieved through a single-detector acquisition setup, which allowed for photo-signal acquisition free from the influence of pulse energy fluctuations, along with intuitive judgement regarding the effects of amplification on both the amplitude and pulse width. An amplification factor of 4.5 for the amplitude, a reduction of 18.4% for the pulse width, and an estimated small signal gain of 0.42% cm<sup>-1</sup> were achieved.

The gain and loss effect during small-signal amplification were theoretically analyzed. The ratio  $\beta$  of the absorption coefficient to the gain coefficient was calculated to evaluate the marginal frequency distortion after amplification. Although the experimental small-signal gain coefficient was not comparable with traditional TEA MOPA systems with narrower linewidth, the spectrum of seed pulses may match the gain spectrum of a CO<sub>2</sub> amplifier at a higher mixture pressure. Moreover, the compression in pulse width after amplification was clarified under the situation without chirping. The absorption loss coefficient by plasma was evaluated as  $-0.26\% \text{ cm}^{-1}$ . Finally, the potential capability of acquiring ultrashort picosecond pulses with ZGP OPO pulses was explored using the FFT function on a modulated spectrum by MATLAB software.

This study is a preliminary attempt to test gain coefficients of new seed sources for LWIR-related amplification research. Because of the limited capability of current devices, there is still much disparity compared with the gain efficiency data of mature facilities in BNL, etc. Further work will be performed after carrying out complete measurements at higher discharge pressures of the amplifier. Amplification of other nonlinear crystal OPO sources, such as a BGSe OPO with a wider tunable range of 9–11 μm, shall also be under consideration. The present study suggests the potential of ZGP OPO as a viable seed source for LWIR amplification systems and provides valuable references for future research in this field.

**Author Contributions:** Conceptualization, Y.Z. and R.T.; methodology, Z.Z., Y.L. and J.B.; software, T.W.; validation, Z.Z.; formal analysis, Z.Z.; investigation, J.T.; resources, Y.Z., J.Y. and X.S.; data curation, J.T.; writing—original draft preparation, Z.Z.; writing—review and editing, R.T. and Z.Z.; visualization, Z.L.; supervision, Y.Z. and X.S.; project administration, Y.Z.; funding acquisition, Y.Z., Z.L. and R.T. All authors have read and agreed to the published version of the manuscript.

**Funding:** This study was funded by the Open-End Fund of the National Laboratory of Science and Technology on Particle Transport and Separation [grant number QT210005] and the National Sciences Foundation of China [grant numbers 61775212 and 61875198].

**Institutional Review Board Statement:** Not applicable.

**Informed Consent Statement:** Not applicable.

**Data Availability Statement:** Data underlying the results presented in this paper are not publicly available at this time but may be obtained from the corresponding author upon reasonable request.

**Conflicts of Interest:** The authors declare no conflicts of interest.

## References

1. Yuan, J.H.; Chen, Y.; Duan, X.M.; Yao, B.Q.; Dai, T.Y. CdSe optical parametric oscillator operating at 12.07  $\mu\text{m}$  with 170-mW Output. *Opt. Laser Technol.* **2016**, *92*, 1–4. [[CrossRef](#)]
2. Yuan, J.H.; Duan, X.M.; Yao, B.Q.; Cui, Z.; Li, Y.Y.; Dai, T.Y.; Shen, Y.J.; Ju, Y.L. Tunable 10- to 11- $\mu\text{m}$  CdSe optical parametric oscillator pumped by a 2.1- $\mu\text{m}$  Ho: YAG laser. *Appl. Phys. B* **2016**, *122*, 202. [[CrossRef](#)]
3. Qian, C.P.; Yu, T.; Liu, J.; Jiang, Y.Y.; Wang, S.J.; Shi, X.C.; Ye, X.S.; Chen, W.B. A high-energy, narrow-pulse-width, long-wave infrared laser based on ZGP crystal. *Crystals* **2021**, *11*, 656. [[CrossRef](#)]
4. Yang, K.; Yao, B.Q.; Li, C.X.; Yao, J.Y.; Mi, S.Y.; Tang, J.W.; Wei, D.S.; Li, J.H.; Hua, X.X.; Duan, X.M.; et al. High efficiency non-critical phase-matching 9.3–10.6- $\mu\text{m}$  optical parametric oscillator in BaGa<sub>4</sub>Se<sub>7</sub> crystal. *Opt. Laser Technol.* **2022**, *160*, 109082. [[CrossRef](#)]
5. Danson, C.; Haefner, C.; Bromage, J.; Butcher, T.; Chanteloup, J.; Chowdhury, E.; Galvanauskas, A.; Gizzi, L.; Hein, J.; Hillier, D. Petawatt and exawatt class lasers worldwide. *High Power Laser Sci. Eng.* **2019**, *7*, e54. [[CrossRef](#)]
6. Haberberger, D.; Tochitsky, S.; Joshi, C. Fifteen-terawatt picosecond CO<sub>2</sub> laser system. *Opt. Express* **2010**, *18*, 17865–17875. [[CrossRef](#)] [[PubMed](#)]
7. Hastings, M.; Panagiotopoulos, P.; Kolesik, M.; Hasson, V.; Tochitsky, S.; Moloney, J. Few-cycle 10  $\mu\text{m}$  multi-terawatt pulse self-compression in a gas-filled multi-pass cell: A numerical experiment. *J. Opt. Soc. Am. B* **2021**, *39*, 266–272. [[CrossRef](#)]
8. Panagiotopoulos, P.; Hastings, M.; Kolesik, M.; Tochitsky, S.; Moloney, J. Multi-terawatt femtosecond 10- $\mu\text{m}$  laser pulses by self-compression in a CO<sub>2</sub> cell. *OSA Contin.* **2020**, *3*, 3040–3047. [[CrossRef](#)]
9. Tochitsky, S.; Pak, A.; Fiuza, F.; Haberberger, D.; Joshi, C. Laser-driven collisionless shock acceleration of ions from near-critical plasmas. *Phys. Plasmas* **2020**, *27*, 083102. [[CrossRef](#)]
10. Kumar, P.; Yu, K.; Zgadzaj, R.; Downer, M.; Vafaei, N.N. Evolution of the self-injection process in long wavelength infrared laser driven LWFA. *Phys. Plasmas* **2021**, *28*, 013102. [[CrossRef](#)]
11. Polyanskiy, M.N.; Pogorelsky, I.V.; Babzien, M.; Kupfer, R.; Vafaei, N.N.; Palmer, M. High-peak-power long-wave infrared lasers with CO<sub>2</sub> amplifiers. *Photonics* **2021**, *8*, 101. [[CrossRef](#)]
12. Polyanskiy, M.N.; Pogorelsky, I.V.; Babzien, M.; Palmer, M.A. Demonstration of a 2 ps, 5 TW peak power, long-wave infrared laser based on chirped-pulse amplification with mixed-isotope CO<sub>2</sub> amplifiers. *OSA Contin.* **2020**, *3*, 459–472. [[CrossRef](#)]
13. Polyanskiy, N.N.; Pogorelsky, I.V.; Babzien, M.; Kupfer, R.; Vodopyanov, K.; Palmer, M. Post-compression of long-wave infrared 2 picosecond sub-terawatt pulses in bulk materials. *Opt. Express* **2021**, *29*, 31714–31725. [[CrossRef](#)]
14. Gordon, D.F.; Hasson, V.; Bergmann, H.V.; Chen, Y.; Schmitt-Sody, A.; Penano, J.R. Advanced concepts for high-power short-pulse CO<sub>2</sub> laser development. In *Ultrafast Bandgap Photonics*; International Society for Optics and Photonics: Bellingham, WA, USA, 2016; Volume 9835, p. 98350Z.
15. Tian, J.T.; Li, Z.Y.; Zhao, L.L.; Liu, S.Y.; Xu, W.N.; Bai, J.Z.; Wu, M.J.; Tan, R.Q. Long-wave infrared ZnGeP<sub>2</sub> optical parametric oscillator with improved tunability by use of a cavity compensation technique. *Opt. Eng.* **2022**, *61*, 076102. [[CrossRef](#)]
16. Smith, K.; Thomson, R. *Computer Modeling of Gas Lasers*; Springer: New York, NY, USA, 2013; p. 337.
17. Wheeler, C.; Fielding, S. Absorption of infra-red radiation as a general technique for the determination of plasma temperature. *Plasma Physics* **1970**, *12*, 551. [[CrossRef](#)]
18. Ginzburg, V.L. *The Propagation of Electromagnetic Waves in Plasmas*; Pergamon: Oxford, UK, 1970; p. 2168.
19. Yablonovitch, E. Self-phase modulation and short-pulse generation from laser-breakdown plasmas. *Phys. Rev. A* **1974**, *10*, 1888. [[CrossRef](#)]

**Disclaimer/Publisher's Note:** The statements, opinions and data contained in all publications are solely those of the individual author(s) and contributor(s) and not of MDPI and/or the editor(s). MDPI and/or the editor(s) disclaim responsibility for any injury to people or property resulting from any ideas, methods, instructions or products referred to in the content.